A snow sensor experiment in Dronning Maud Land, Antarctica

Hardy B. GRANBERG,[1] Patrick CLICHE,[1] Olli-Pekka MATTILA,[2,*] Eija KANTO,[2] Matti LEPPÄRANTA[2]

[1]*Centre d'Applications et de Recherche en Télédétection (CARTEL) and Département de Géomatique Appliquée (DGA), Université de Sherbrooke, Sherbrooke, Québec J1K 2R1, Canada*
[2]*Department of Physics, University of Helsinki, PO Box 64, Gustaf Hällströmin Katu 2, FIN-00014 Helsinki, Finland*
E-mail: matti.lepparanta@helsinki.fi

ABSTRACT. In January 2000 nine snow sensors were deployed in Dronning Maud Land, Antarctica, along a 355 km transect from Kvitkuven near the shelf edge via the Finnish research station, Aboa, to the Amundsenisen plateau. The purpose was to test a sensor system for spatio-temporal variations in temperature across the snow–air interface and snow accumulation/ablation, which includes atmospheric net balance and migrating snow dunes. In the dry snow conditions, environmental static electricity interfered with data transfer; several sensors were disabled early, while the longest record reached 6 months. Along the main transect, the year 2000 mass balance ranged from 52 to 221 mm w.e., largely following spatial patterns seen by other researchers. The level increased toward the edge of the ice sheet; unloading of drifting snow as the slope flattens, rather than increased snowfall as previously thought, may be responsible for this. At the Högisen ice dome site the mass balance was 897 mm w.e., possibly due to unloading of wind-blown snow, as katabatic winds are locally forced uphill. This mechanism is important to maintain such topographic features along the Antarctic ice sheet margin. Major precipitation events occurred at 3–5 week intervals and much of the precipitation fell before mid-June. The daily signal in temperature disappeared after the autumn equinox, then the spectrum displayed a broad peak at synoptic frequencies. Potential temperature decreased towards the shelf edge, displaying a pattern consistent with strong inversions and suggesting that strong evaporative cooling is associated with the katabatic winds.

1. INTRODUCTION

The vast snowfields of Antarctica influence the world's climate in ways that are not well understood at present. The mechanisms which keep the 70 m sea-level equivalent of snow and ice from melting are also unclear. This lack of understanding is disquieting in a world of rapidly rising atmospheric CO_2 levels and predictions about consequent polar warming. Snow properties readily respond to changing environmental conditions, and, as they become buried by new snow, individual snow layers record past weather and cumulative climate conditions. To better relate signals observed by satellite remote sensing and data from ice cores to environmental conditions, we need more information about the snow surface layer, in particular spatio-temporal variations in snow mass balance and temperature.

The time snow spends at the surface is an important determinant of its properties. In newly deposited snow, large micro-scale variations in surface tension drive intergranular bonding and a rapid reduction of specific surface area. Absorption of solar radiation, terrestrial radiation balance and sublimation can generate steep temperature gradients, which, together with wind pumping, drive rapid metamorphism. Dust fall adds further environmental information, and photochemical processes contribute their signatures. It is at the snow surface that isotope ratios and the concentrations of contaminants may be altered by snowdrifting, sublimation and melt/freeze cycles. Thus, the net accumulation rate and the variability of the surface environment are important to the development of realistic conceptual and numerical models. Such models are useful in remote-sensing assessment of snow and ice sheets and are key to the understanding of Antarctica's current and past relationships with global climate.

As part of an earlier snow-cover modelling project (Granberg and Irwin, 1990) a snow sensor system was developed for high-time-resolution data on net accumulation and temperature of snow. It proved useful in driving and calibrating simple spatial snow-cover models. During the Finnish Antarctic expedition to Dronning Maud Land in the austral summer 1999/2000 (FINNARP 1999), nine such snow sensors were deployed at ~60 km spacing along a transect (Fig. 1) from Kvitkuven, near the shelf edge, to a point on the Amundsenisen high plateau. They were retrieved a year later. The research station Aboa served as the field base, situated on the Basen nunatak (73°03′ S, 13°24′ W), ~125 km inland from the shelf edge.

The purpose of this installation was two-fold. First, it was a field test of these sensors in a new and challenging environment. Although earlier prototypes have been successfully field- tested at Schefferville (55° N, 67° W) and near Sherbrooke (45° N, 70° W) in Canada, Antarctica offered new challenges with regard to the physical environment and the logistics of sensor deployment and retrieval. A second purpose was to derive information on the timing, magnitude and spatial extent of snow-accumulation events and to examine the microclimate, focusing on the thermal regime, which is strongly influenced by the katabatic outflow from the Antarctic interior (Van den Broeke and others, 1999). This outflow has consequences for the regional climate as it adds wind velocity to the Antarctic anticyclone.

*Present address: Finnish Environment Institute, PO Box 140, FIN-00251 Helsinki, Finland.

https://doi.org/10.3189/002214309790794823 Published online by Cambridge University Press

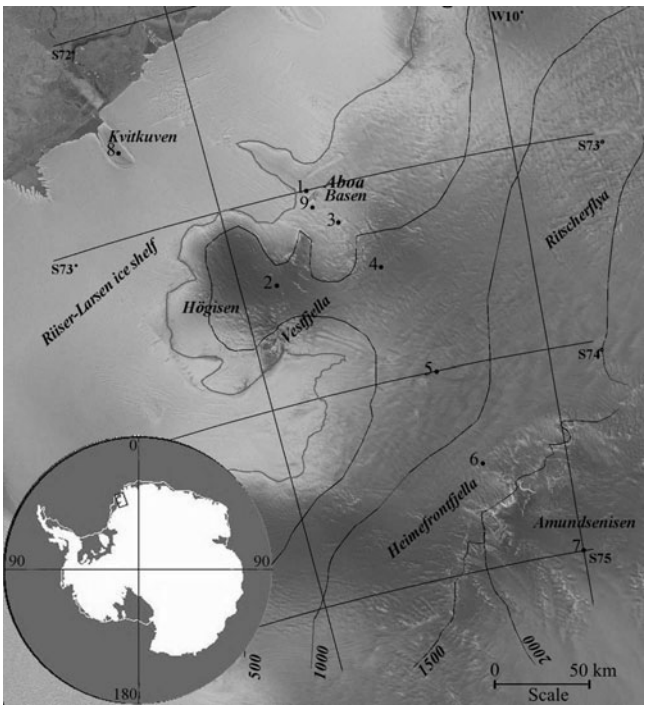

Fig. 1. Map of the study region with the snow sensor locations indicated. The background is part of a RADARSAT mosaic from the region (© Canadian Space Agency 1997), with the geographic grid and elevation contours superimposed (source: maps of Norwegian Polar Institute). Also shown are the Dutch automatic weather stations AWS 4 and AWS 5 (Reijmer, 2001).

The spatial variations of snow accumulation in the Dronning Maud Land sector are now relatively well known, through stake surveys, firn cores and radar profiling (Isaksson, 1992; Isaksson and Karlén, 1994a,b; Isaksson and others, 1996; Richardson and others, 1997; Kärkäs and others, 2002; Richardson-Näslund, 2004). Relationships between the spatial variations in snow accumulation and the katabatic outflow have long been recognized (Gow and Rowland, 1965) and have been further elucidated by ground-probing radar profiles and firn cores, but they are still poorly understood (Melvold and others, 1998), particularly on an event-by-event basis. Consequently, a more detailed quantitative understanding of the spatio-temporal aspects of accumulation is desirable. This would improve Antarctic mass-balance estimates, serve as validation for regional climate models (e.g. Van Lipzig and others, 2002a,b) and reduce the uncertainties in our interpretation of the information contained in Antarctic ice cores, which provides much of our understanding of past climate variations (e.g. Petit and others, 1999; EPICA Community Members, 2004). A sparse network of micrometeorological stations, which also monitor snow depth, has been in operation for some time in Dronning Maud Land and elsewhere in Antarctica (Reijmer and Van den Broeke, 2003). The spatio-temporal variations recorded to date show the need for a much denser network of sensors capable of synchronized monitoring of air temperature and snow depth.

This paper describes the FINNARP snow sensor experiment and its results. The field area and the sensors are described below. Then the logistics of sensor installation and retrieval are detailed, and sensor data and auxiliary field measurements are analysed. Although some technical problems were encountered, the utility of the sensors for automated snow monitoring was ultimately successfully demonstrated.

2. MATERIAL AND METHODS

2.1. Snow sensors

Each snow sensor (Fig. 2) consists of a 15 mm diameter rod, 1.2 m long, with thermal sensors positioned along it at 2 cm intervals. Sensor calibration prior to the experiment resulted in accuracy better than 0.2°C, and the resolution of both successive temperature measurements and those along the sensor rod are well within 0.1°C. To minimize radiation errors, the sensor rod is high-reflectance white plastic with radiant emission properties close to that of a black body. Nevertheless, some radiation error may occur in calm conditions with strong sunshine. The absolute daytime temperatures may be biased, but the night temperatures allow snow-surface identification. The sensor rod is affixed to a cylindrical housing, made from 4 in (100 mm) diameter acrylonitrile butadiene styrene (ABS) plastic tubing, which houses a data logger. The version employed here can record twice-daily measurements from each thermistor for a period of 15 months (a new prototype version is now capable of many years of data acquisition at 10 min intervals). Programming and data retrieval are via an RS232 interface with cable extension; satellite data transmission was not designed due to financial limitations.

The sensor itself is built to withstand Antarctic winter temperatures. However, the alkaline batteries of the power supply cannot deliver the necessary current at temperatures below about –40°C. In earlier applications the sensor was installed in the soil, with the top of the housing positioned level with the surface. The housing itself was longer, containing a battery pack in its lowest part, protecting it from extreme low temperatures. In the version discussed here, we used a 4 m long insulation-filled installation tube with batteries in the bottom (Fig. 2). There the batteries would be exposed to temperatures within ~4°C of the annual average air temperature (Schytt, 1960), which at Aboa is –15.3°C, based on weather station records from 1989 to 2001 (Kärkäs, 2004). To facilitate retrieval, we used PVC tubes with a glossy exterior finish. To satisfy Antarctic environmental protection requirements, the battery pack was attached to an internal glass-fibre strap to enable it and the insulation to be retrieved separately, should steam heating be needed to free the pipe.

2.2. Sensor locations and installation

The sensor rods were installed along a 355 km long transect (Fig. 1), covering the entire katabatic zone from a point near 75° S, 10° W on the Amundsenisen high plateau to Kvitkuven (72°22′ S, 16°49′ W) near the shelf edge. Snow conditions along this transect are well known from previous firn-core and isotope studies (Isaksson, 1992; Isaksson and Karlén, 1994a b; Isaksson and others, 1996) and snow-radar and accumulation-stake surveys (Richardson and others, 1997; Richardson-Näslund, 2004).

From Amundsenisen, at the southeastern end of the transect, the ice sheet descends steeply from an altitude of ~2900 m to 1100 m just below the Heimefrontfjella mountain range, which impedes the ice flow. Thereafter the

https://doi.org/10.3189/002214309790794823 Published online by Cambridge University Press

descent is much gentler to an altitude of ~900 m ~50 km southeast of Aboa, where the ice-surface slope steepens towards the grounding line of the Riiser-Larsen Ice Shelf near Aboa. The ice shelf northwest of Aboa floats and is therefore expansion-crevassed, sloping gently from an elevation of just over 200 m near Aboa to <50 m at the top of the shelf edge. (For more details about the field area, see, e.g., Jonsson, 1988; Holmlund and Näslund, 1994; Rasmus and others, 2003.)

The sensors were installed on open snowfields that were relatively flat and without crevasses for at least a 3 km radius, to minimize the effects of locally differential snow transport. Their positions were selected to represent a gradation in altitude and distance from the sea (Table 1). However, two deviations were made from our original sampling plan. Sensor 2 was installed off the main transect, on Högisen ice dome, to examine a local low-backscatter anomaly in the RADARSAT Antarctic mosaic shown in Figure 1. Sensor 8 was installed on Kvitkuven with the intent of installing sensor 9 on the shelf edge nearby for comparative measurements, but this plan had to be abandoned and sensor 9 was installed near Aboa station instead.

2.3. Installation and retrieval procedure

At each site a pit ~0.5 m deep was dug. A SIPRE/CRREL corer was employed to drill a hole to ~4.3 m depth below the snow surface. The battery pipe was inserted into this hole and seated with its upper rim slightly below the surface. The snow sensor was inserted into the pipe, flush with its upper rim, and the top of the pipe was sealed using conventional plastic kitchen wrap to prevent moisture from entering. At this stage, the sensor was programmed by means of a portable computer. Subsequently, the RS232 cable was wound around the top part of the pipe, sealed with additional wrap, the snow pit was backfilled and the surface was then levelled to approximate the original surface. The coordinates were recorded using the global positioning system (GPS). Flagged bamboo poles, ~3.5 m long, were added to facilitate finding the sensors. Twice-daily temperature profiles were measured synchronously by all sensors at 0600 and 1800 GMT (the solar noon is within 1030–1130 GMT here).

After 1 year, sensor retrieval was mostly straightforward (Fig. 2). The flagged poles marking each site were easily spotted once the sensor site had been generally located by GPS-directed snowmobile. The snow-surface level with respect to the top of the sensor rod was noted. No influence of the sensor rod on nearby snow accumulation could be seen. A pit was excavated around the sensor, the data were dumped to a portable computer and the battery pipe was extracted. Data transfer in the field was unexpectedly difficult. In the dry snow conditions typical of the area, environmental static electricity interfered with the transfer, causing interruptions. The datasets were subsequently successfully retrieved in the better-grounded indoor environment at Aboa. However, a similar problem had also affected data collection. In the seven sensors that were still operational at the time of retrieval, the data loggers had all reset at some stage during the winter, and two sensors had been disabled. The dataset is therefore incomplete (Table 1). In general, it appeared that in the milder Antarctic coastal climate the sensors functioned better than in cold and dry conditions.

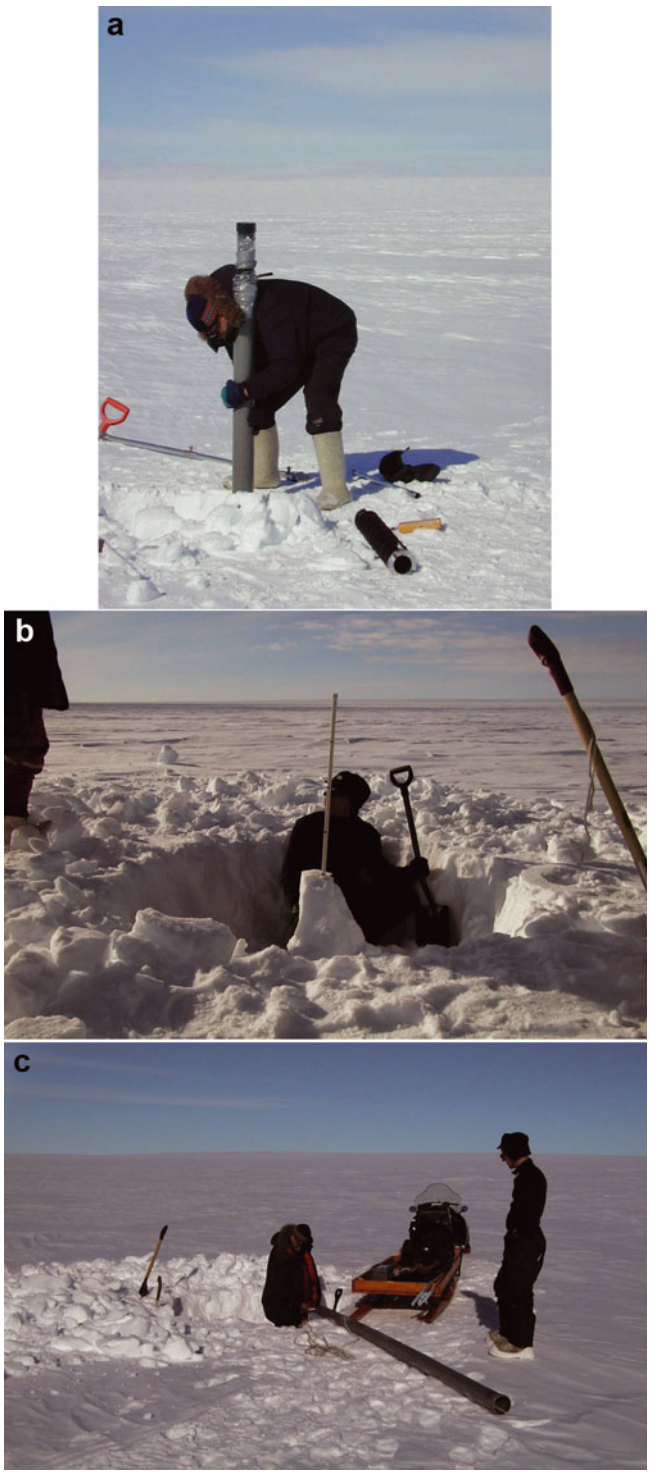

Fig. 2. (a) Deployment of the battery pipe. (b) Digging the snow around the sensor rod for retrieval. (c) The batteries used in the bottom of the pipe to supply power. (Photographs: E. Kanto.)

2.4. Temperature data

Upon both sensor installation and retrieval, a snow stratigraphic analysis was made in a separate pit nearby (Kärkäs and others, 2002, 2005; Rasmus and others, 2003). Snow density and temperature profiles (4.3 m deep) were measured using the core extracted during the installation of the battery tube at each site (Fig. 3). The densities were measured by weighing 10–30 cm thick core slices, and the temperatures were measured using a digital thermometer (EBRO TLC1598) fitted with a 0.1 m long, 3 mm diameter

https://doi.org/10.3189/002214309790794823 Published online by Cambridge University Press

Table 1. Locations of snow sensors 1–9. Also shown are the altitude, distance from the shelf edge, start and end of the collected data file, and temperature and potential temperature at installation at 4.3 m depth. The potential temperature is given with respect to the sea-surface pressure

Sensor	Latitude (W)	Longitude (S)	Altitude	Distance	Start	End	Temperature	
					(day of 2000)		In situ	Potential
			m	km			°C	°C
1 Aboa1	72°57.859′	13°34.560′	270	110	004	085	–17.4	–14.7
2 Högisen	73°26.222′	14°26.723′	990	130	006	—	–17.3	–7.7
3 Basen, south	73°12.500′	13°12.996′	375	140	008	053	–16.3	–12.6
4 Vestfjella	73°27.362′	12°33.381′	905	170	010	116	–21.2	–12.3
5 74°S	74°00.794′	12°01.129′	980	230	012	038	–20.3	–10.7
6 Heimefrontfjella	74°28.688′	11°33.006′	1100	275	014	075	–22.3	–11.5
7 Amundsenisen	74°59.866′	10°00.485′	2900	355	014	—	–37.0	–8.6
8 Kvitkuven	72°36.546′	16°18.601′	280	15	018	168	–16.0	–13.3
9 Aboa2	73°04.085′	13°28.225′	235	125	028	046	–16.0	–13.7

probe, which was inserted into the bottom of each core length immediately after extraction; the accuracy is 0.2°C. It is assumed that the monthly snow density profiles are the same from year to year, making it simple to transform net snow accumulation into mass balance. There are small variations due to differences in snowfall and temperature history in different years, but they have only minor influence on the mass-balance estimation.

The time series of the position of the snow surface was determined from the temperature profile records. Snow depths were visually estimated and digitized from screen plots using the screen cursor. As in the earlier Canadian tests, the snow-surface level was almost always identifiable from the temperature gradient (Fig. 4). The estimation becomes clearer in the time-series data since it is usually easy to follow the evolution of the temperature profiles in snow and air and, consequently, the point where they meet (surface). In the few cases when it was not identifiable, the depth was estimated using the previous and succeeding estimates. The estimated accuracy of the surface level is about the thermistor interval of 2 cm in the rod.

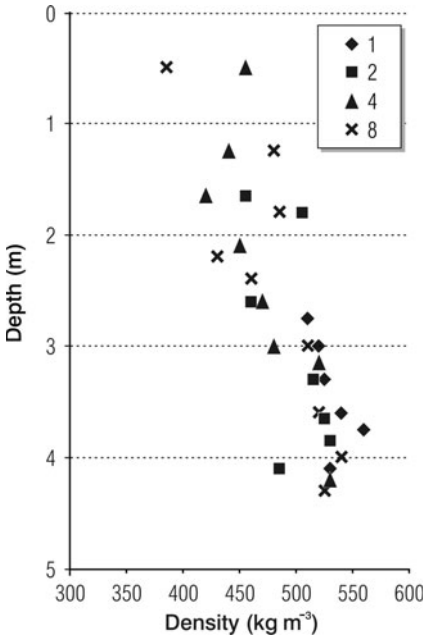

Fig. 3. Snow density profiles for four snow sensor sites (1, 2, 4 and 8) measured at the time of installation from 10–30 cm thick firn-core slices.

According to Aboa weather station data, the monthly mean air temperature ranges from –5.2°C in January to –21.9°C in August (Kärkäs, 2004). In the snowpack the amplitude of temperature variation is attenuated with depth; for the annual cycle the *e*-folding depth is ~4 m for snow with 400 kg m^{-3} density (see, e.g., Paterson, 1994). Schytt (1960), working on the ice shelf at Maudheim, northwest of Aboa, gave the annual amplitude as ~6°C at 4.3 m depth. His data at this depth further showed that in January the temperature range is 2°C and in mid-January the temperature nearly equals the annual mean. Consequently, our January temperatures from the bottom of the drill cores should be within ~1°C of the annual average air temperature.

The average annual potential temperatures were estimated assuming an average dry adiabatic lapse rate of 9.8°C km^{-1} and using the 4.3 m temperature (Table 1). These potential temperatures are with respect to sea level, not the usually assumed 100 kPa sea-level pressure. The average annual sea-level pressure is 98.76 kPa at Aboa and 98.64 kPa at Neumayer (70°37′ S, 8°22′ W), a nearby station at the shelf edge (Kärkäs, 2004). Therefore, for approximate conversion to 100 kPa reference, simply add 1°C.

3. SNOW ACCUMULATION

3.1. Annual mass balance at the sensor sites

The annual mass balance of snow at each site was obtained from the snow measurements at installation and retrieval of the sensors. It was necessary to correct the observed snow depths for the zero offset (when the sensor rods were deployed, the reference mark was left slightly below the surface, so the unbiased initial snow-surface level was obtained using the thermistor chain), timing (the results were standardized to represent the period 4 January 2000 to 4 January 2001, i.e. very nearly the calendar year 2000), and snow compaction over the 4 m long installation pipe. The temporal depth variations measured by the snow sensors (Fig. 5) and the density profiles measured during sensor installation (Fig. 3) allowed us to perform these operations (Table 2). The correction for zero offset was straightforward

https://doi.org/10.3189/002214309790794823 Published online by Cambridge University Press

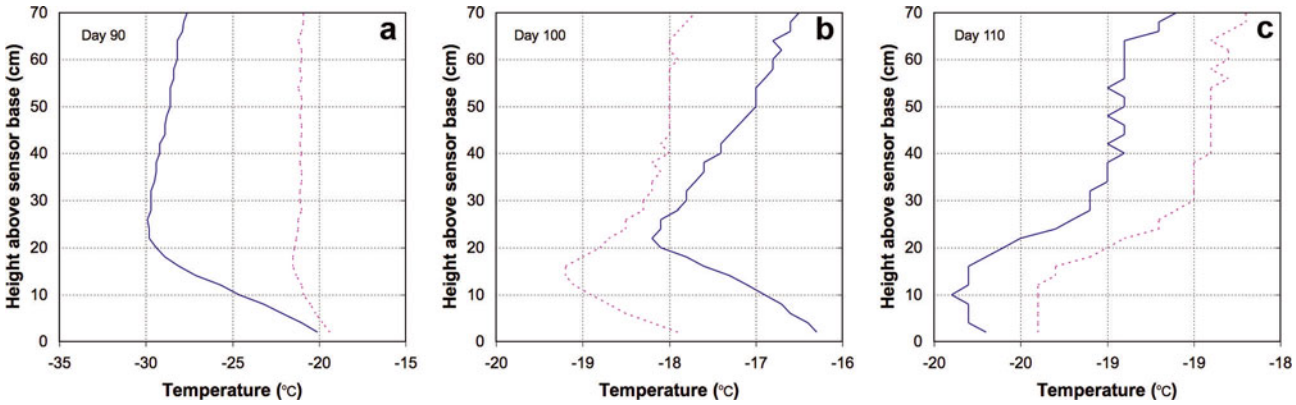

Fig. 4. Temperature profiles at snow sensor site 8 for days 90 (a), 100 (b) and 110 (c); 0600 GMT (solid curve) and 1800 GMT (dashed curve). Day 90 shows snow surface at 20 cm, identifiable only in the morning profile; day 100 has snow surface still at 20 cm, with temperature inversion, and day 110 has snow surface at 30 cm.

in all but two cases. The first snow depths recorded by the sensors were taken as the zero depth upon installation. For the two disabled sensors it was supposed that the zero offset was similar for all sensor installations (it varied from 10 to 18 cm), and we employed the average value of 13 cm.

The timing correction was based on the sensor data from January, or for the disabled sensors the average January net accumulation rate. In general, the evolution of the surface elevation, H, with respect to the level at a fixed time can be expressed as

$$H(t+\Delta t) = H(t) + [S(t+\Delta t) - S(t)] - [L(t+\Delta t) - L(t)], \quad (1)$$

where S is accumulation, L is ablation, t is time and Δt is time change. This way the observations can be rendered comparable with each other. Here accumulation and ablation include the migration of snow dunes that is of major concern to sensor registration heights. The sensor sites, apart from Högisen ice dome, were, however, chosen from large even areas where the net influence of the migrating dunes is expected to be small over long timescales.

In January 2000, there were a few minor precipitation events (Fig. 5). Sensor 1, which was installed first, recorded these events near Aboa as an elevation increase of ~3 cm on 14 January, while sensor 3, also near Aboa, reacted less to them indicating an increase of ~2 cm followed by a decrease (not shown). Sensor 1 showed an increase of ~3 cm on 23–24 January, giving a total of 6 cm since 4 January. Sensor 4, installed on 10 January on the eve of a snowstorm, gave an increase of 6 cm in the period 10–12 January then remained fairly steady for the remainder of the installation period. Snow depths varied over a range of ~4 cm, probably as a result of shallow migrating sastrugi driven by the wind. Sensor 5 (not shown) had an increase in depth of ~8 cm from 12 to 13 January and thereafter a decline to ~3 cm above the zero offset, taken here as 10 cm. Overall, the change in depth during the installation period of all the sensors (4–28 January) was small; a 3 cm correction is estimated applicable for the sensors installed on 14 January or later. In addition, sensor 9, installed on 28 January, has been corrected by –6 cm for net evaporative losses. For the period of snow sensor retrieval, no corrections were deemed necessary.

The compaction of snow was determined from the density profiles. These were quite similar at the installation sites (except for Amundsenisen and Högisen (sensors 7 and 2)), with a surface density of ~400 kg m^{-3} and a density of ~570 kg m^{-3} at 4 m depth. The evolution of the snow depth, h, follows the equation

$$\frac{dh}{dt} = -\gamma h + d', \quad (2)$$

where t is time, $\gamma < 1$ is the compaction rate and d' is the net accumulation rate. With d' and γ as constants and $h(0) = 0$, the solution is

$$h(t) = d't\frac{1 - \exp(-\gamma t)}{\gamma t}. \quad (3)$$

Taking γ as a constant limits the applicability of the solution to a surface layer <10 m thick. This model produces an approximately linear density profile across the top 4 m snow layer, in good agreement with measured densities (Fig. 3).

At the sensor sites, except Amundsenisen and Högisen (sensors 7 and 2), the mean and standard deviation of annual net accumulation were 43 and 5 cm, respectively, so 4 m depth represents ~10 years mass balance. The density data gave a total compaction by a factor of 0.85 for the 4 m deep snow column. The compaction rate can be numerically found using $[1 - \exp(-\gamma t)]/(\gamma t) = 0.85$ at t = 10 years, resulting in γ = 0.033 a^{-1}. On Amundsenisen, the 4 m depth interval represents >20 years mass balance; the density was 500 kg m^{-3} at 4 m depth, and thus γ = 0.011 a^{-1}. On

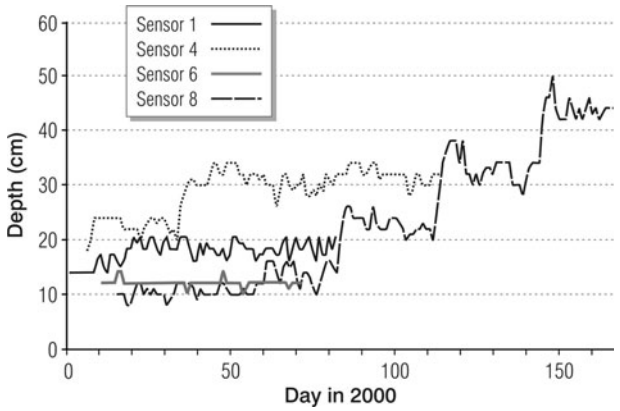

Fig. 5. Snow-depth time series measured by sensors 1, 4, 6 and 8. (Sensors 2 and 7 were disabled at the start and recorded no data; sensors 3, 5 and 9 have only short records.)

https://doi.org/10.3189/002214309790794823 Published online by Cambridge University Press

Table 2. The mass balance of snow in 2000. Recorded change gives the apparent mass balance with respect to the sensor rod. The corrections shown are due to zero point offset, accumulation/ablation due to timing difference from the standard year, and compression across the layer of the sensor rod depth. Mass balance represents the corrected estimate, and the final column gives the corresponding water equivalent

Sensor	Installed	Retrieved	Recorded change	Correction			Mass balance	
				Zero offset	Timing	Compression		
			cm	cm	cm	cm	cm	mm w.e.
1	4 Jan. 2000	3 Jan. 2001	45	–14	0	13	44	180
2	6 Jan. 2000	13 Jan. 2001	184	–13	0	40	211	897
3	8 Jan. 2000	2 Jan. 2001	41	–17	0	13	37	151
4	10 Jan. 2000	13 Jan. 2001	47	–18	0	13	42	172
5	12 Jan. 2000	12 Jan. 2001	38	–10	0	13	41	167
6	14 Jan. 2000	12 Jan. 2001	35	–12	3	13	39	159
7	14 Jan. 2000	12 Jan. 2001	19	–13	3	4	13	52
8	18 Jan. 2000	20 Jan. 2001	48	–10	3	13	54	221
9	28 Jan. 2000	31 Dec. 2000	48	–12	–6*	13	43	176

Note: There was no significant snowfall during the period of sensor retrieval in 2001.

Högisen, the time is only 2.2 years, and with the density of 500 kg m^{-3} at 4 m depth we have $\gamma = 0.10\,\mathrm{a}^{-1}$. This case agrees well with the type of sensor damage that occurred and with the compressed state of the sensor installation pipe that was observed upon excavation.

When the compression factor, γ, has been obtained, Equation (2) can be used to accurately estimate the annual mass balance by $d' = \mathrm{d}h/\mathrm{d}t + \gamma h$. The results, neglecting the values for sensors 2 and 7, are 37–54 cm, corresponding to 151–221 mm w.e. For sensor 2 (Högisen) and sensor 7 (Amundsenisen) the results were 211 cm and 897 mm w.e., and 13 cm and 52 mm w.e., respectively (Table 2). There was a trend for decreasing annual mass balance inland from the shelf edge, with Högisen as a notable exception. Local variations were less important, as illustrated by the three sensors in the vicinity of Aboa: for sensors 1, 3 and 9, the annual mass balances were 44, 37 and 43 cm, respectively (Table 2). This range of only 7 cm is well within the local snow-depth variation due to snow dunes.

At all sites several thin ice lenses were identified in the snow pits in the top metre, and south from Aboa a depth-hoar layer was found, except at site 5 (Rasmus and others, 2003). In Amundsenisen the ice lenses were very thin and two depth-hoar layers were found. In Högisen the snow was softer than in the ice shelf and almost no ice lenses were seen, and the observed compression of the installation pipe was therefore caused by the high accumulation rate.

3.2. Snow accumulation history in a balance year

The snow-depth time series were longest for sensors 8, 4 and 1 (Fig. 5). In January 2001 the depths on sensor retrieval were 48 cm for sensor 8, 47 cm for sensor 4 and 45 cm for sensor 1. On day 35 there was a rapid snow-depth increase of 10 cm at sensor 4, but, other than that, the records show only short-term variations around a mean level until day 80. Thereafter, sensor 8 experienced three main accumulation events at 3–5 week intervals. The snow depth observed on sensor retrieval was equalled by day 160, just before the Antarctic winter solstice.

Thus the results from sensor 8 (located on Kvitkuven, close to the shelf edge) suggest that much of the annual precipitation arrives in the first half of the calendar year. This agrees with modelling results of Van Lipzig and others (2002a b). Sensors 8 and 4 together further suggest that precipitation arrives in discrete major accumulation events. Depending on the degree of fragmentation of snow crystals due to the wind, the initial snow density is 200–400 kg m^{-3} (Kotlyakov, 1966). At sensor 8 this represents 15–60 mm w.e. delivered by each main accumulation event. Reijmer and Van den Broeke (2003) examined snow accumulation in the same region using automatic weather stations. At their station AWS 5 (73°06.3′ S, 13°09.9′ W; Fig. 1) the accumulation pattern was similar, i.e. a few large accumulation events in the early part of the winter. However, at their station AWS 4 on the ice shelf (72°45.2′ S, 15°29.9′ W; Fig. 1), snow accumulation was semi-continuous through numerous smaller accumulation events. This suggests that their AWS 4 experienced unloading of snow by katabatic winds as the surface slope flattened on the shelf, but that their AWS 5 and our sensor 8 did not experience such differential drift transport.

A prominent feature in sensors 4 and 8 is the fairly rapid decline in snow depth, usually ~5 cm or more between snowfalls. This is partly because the sensor records depth compaction over the entire length of the installation pipe plus the depth measured by the snow sensor rod. This snow layer experiences a rapid initial adjustment of the snow cover to the new load. A part of the decline is also caused by the strong initial effects of surface tension, as well as fragmentation and packing of snow particles by the strong winds usually accompanying snowfall in this area. No signs of the rods being a snow obstruction were noted at the time of the recovery.

Features of rapid rise and decline in snow depth are also seen in the data of Reijmer and Van den Broeke (2003), some of a more extreme nature than those observed here; their cause may be different, possibly related to the passage of snow dunes through the sensor location. Our datasets showed no such events, possibly due to the method of surface tracing, but the more extensive datasets of Reijmer and Van den Broeke (2003) have captured a few. Outside such events, the depth decline in excess of that attributable to depth compaction is the result of mass loss through snow abrasion and through the subsequent, often airborne, evaporation of that snow.

https://doi.org/10.3189/002214309790794823 Published online by Cambridge University Press

With the extremely dry air drawn from the stratosphere by the Antarctic anticyclone, mass loss by evaporation can be important even at low winter temperatures, but is, of course, particularly important in summer. Between 10 December 2004 and 24 January 2005, 79 ± 24 mm w.e. evaporated from the glacier near Aboa, as determined by stake-line measurements (Kanto and others, 2007). This represents an average snow-surface elevation decline of 0.45 cm d^{-1} due to evaporation, assuming a surface layer density of 400 kg m^{-3}. The depth compaction rate was <0.04 cm d^{-1} (apart from sensor 2 at Högisen), and therefore 0.4 cm d^{-1} (1.6 mm w.e. d^{-1}) is estimated as the summertime evaporation rate. For most sites, there was only a deviation of a few days between the measurement year and 365 days (Table 2). Therefore no correction has been made for evaporation, except for sensor 9, where the measurement year started late (28 January 2000). Hence 6 cm snow depth was subtracted for the net accumulation, bringing the corrected depth to 36 cm (148 mm w.e.). This sensor is located near the stake-line where the evaporation rates were measured.

There are significant variations in the amount of snow deposited by individual storms. Sensor 4 (Fig. 5), ~170 km from the coast, experienced a snowstorm which started on day 38, adding ~12 cm over the following 4 days. This storm only deposited 3–4 cm of snow at sensor 8, near the coast, and similarly insignificant amounts elsewhere. By contrast, the storm near day 80 only added ~6 cm at sensor 4, while at sensor 8 >20 cm accumulated. These fairly steep spatial variations in snowfall may be a characteristic of the high-latitude, polar-type cyclones responsible for the bulk of the polar precipitation, but they may also be the result of local factors. Antarctic snowfall usually forms migrating dunes, and the accumulation measured in one storm depends on the precise location where a dune stabilizes in relation to the snow sensor. A stable dune hardens and becomes a topographic roughness element on which the next snowfall accumulates. A large snow-depth increment may therefore be registered from a modest snowfall, or even from a mere snowdrifting event.

3.3. Annual snow accumulation in the study region

At first glance we note a fairly uniform snow accumulation with distance from the shelf edge. At the edge (sensor 8) the net accumulation was 221 mm w.e., declining to 180 and 176 mm w.e., respectively, for sensors 1 and 9, located near Aboa. At sensor 3, 140 km from the shelf edge, the accumulation diminished to 151 mm w.e.; this site is at an altitude of 375 m, located in the lower part of the section, where the glacier is thinning as it approaches the grounding line. Above this slope, the accumulation was greater: sensor 4 (altitude 905 m, distance 170 km) had 172 mm w.e. and Sensor 5 (altitude 980 m, distance 230 km) had 167 mm w.e. At sensor 6, located below the steep glacier descent near Heimefrontfjella, the accumulation was again lower, 159 mm w.e. Beyond Heimefrontfjella, on Amundsenisen (sensor 7, 355 km inland) the accumulation became sharply lower, 52 mm w.e., but with some uncertainty because of the indirectly estimated zero offset. At sensor 2 on Högisen, the accumulation was 897 mm w.e., some five times that observed at other stations nearby. The three sensors geographically closest to Aboa (1, 3 and 9) accumulated 151–180 mm w.e.

In FINNARP expeditions, snow accumulation was also examined from snow pits (Kärkäs and others, 2005). The mean net accumulation was 318 mm w.e. on the ice shelf, 218 mm w.e. after the grounding line and 92 mm w.e. on the plateau. The present snow-sensor results are lower, but Kärkäs and others (2005) found an interannual variability of ±50 mm w.e. It is difficult to distinguish annual layers in snow pits in this transect because of the general lack of surface melt crusts and the presence of subsurface melt features.

In general, our observations compare well with previous reports from Dronning Maud Land. Amundsenisen (sensor 7) is characteristic of the accumulation regime of the interior high-polar plateau of East Antarctica, where a large part of the accumulation consists of rime deposits and ice crystals condensing out of the very dry air that descends into the Antarctic anticyclone. The net accumulation of ~52 mm w.e. in year 2000 is similar to results for the interior plateau reported by Van den Broeke and others (1999, table 1) who reported values ranging from 24 to 59 mm w.e. for stations located at distances of ≥300 km from the shelf edge. However, our 52 mm w.e. is much lower than the ~90 mm w.e. found by Isaksson and Karlén (1994b, fig. 6) and by Richardson-Näslund (2004, fig. 2). Although our net accumulation rates are consistently smaller, the patterns of net accumulation from Amundsenisen towards the shelf edge agree well with those of Richardson-Näslund (2004, fig. 2).

The accumulation rates in the coastal parts of Richardson-Näslund's radar transect, at AWS 4 and on Högisen ice dome were quite large. It is likely that they are the result of unloading of wind-blown snow by the katabatic outflow. This outflow decelerates, and expansion cools as it ascends the ice dome and may thus generate precipitation in addition to unloading. At the toes of steeper slope segments, including their entry onto the flat surface of the ice shelf, there is also such unloading. At Kvitkuven, well away from the shelf grounding line, the unloading of wind-blown snow by the katabatic outflow has become insignificant, so Kvitkuven should be fairly representative of local snowfall. If so, then the shelf edge/inland gradient of snow accumulation reported by several authors may be, at least partly, the result of coastwards snowdrift transport, and the precipitation gradient is perhaps less important than previously thought.

4. SNOW TEMPERATURE

4.1. Temperatures at 4.3 m depth and potential temperatures

The temperatures taken at the bottom of the 4.3 m snow cores show a large spatial variation, ranging from –16.0°C at sensor 8, near the coast, to –37.0°C at sensor 7 on Amundsenisen (Table 1). In the vicinity of Aboa, sensors 1 and 9 show temperatures of –17.4 and –16.0°C, respectively, while the long-term (1989–2001) annual average air temperature at the Aboa automatic weather station (AWS) is –15.3°C (Kärkäs, 2004). Aboa AWS is located at an altitude of 484 m while the altitudes of sensors 1 and 9 are 270 and 235 m, respectively. The difference in temperatures between them and Aboa AWS suggests that the temperatures measured on the nunatak are, on average, ~1.4°C higher than that for the glacier below, presuming our two assumptions based on Schytt's (1960) results are valid: at 4.3 m depth, in January the temperature range is 2°C and in mid-January the

https://doi.org/10.3189/002214309790794823 Published online by Cambridge University Press

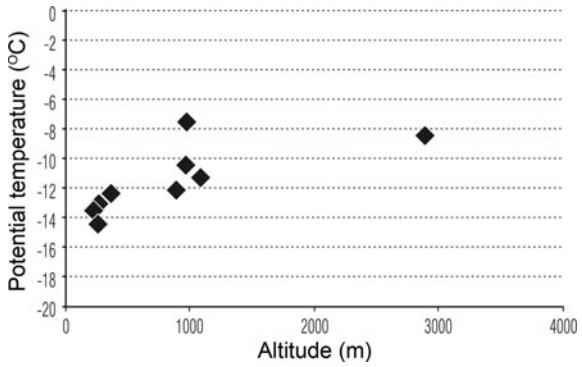

Fig. 6. Annual average potential temperature vs elevation along the Aboa transect. The values of the points are given in Table 1.

temperature nearly equals the annual mean. This would suggest that, aside from local heating effects discussed by Kärkäs (2004), there are, on average, temperature-inversion conditions in this part of the katabatic zone. The data further show that the inversion becomes stronger in autumn and winter.

On Högisen (sensor 2) the temperature was –17.3°C, close to that for sensors 1 and 9 near Aboa, although the elevation is higher by 720 and 755 m, respectively, and accordingly the potential temperature is –7.7°C, warmer by 6 and 7°C than on the ice sheet near Aboa. Part of this increase in potential temperature with altitude may be due to condensation in the ascending katabatic layer mentioned earlier, but there is also a highly stable atmospheric stratification associated with the katabatic outflow regime (Fig. 6).

Aside from Högisen (sensor 2), Amundsenisen (Sensor 7) has the highest average annual potential temperature (–8.6°C). Net radiation cooling and cooling by snow evaporation are the two mechanisms that lower the potential temperature gradually towards the coast. The first is a function of the atmospheric thermal radiation and surface temperature. The second depends on the water vapour deficit and the wind speed, both of which are related to surface slope in this setting. Sensor 1, located at a distance of 110 km from the coast, shows the lowest potential temperature (–14.7°C). The most pronounced lowering of potential temperature occurs in association with the steepest surface slope segments, suggesting that evaporation of snow associated with the katabatic outflow is an important mechanism contributing to the lowering of the potential temperature of the near-surface air.

Based on the results at Högisen (sensor 2), the –13.3°C potential temperature at sensor 8, located on the Kvitkuven ice rise, is ~2°C greater than might be measured on the nearby ice shelf, ~200 m below. Under this assumption, potential temperature declines all the way to the coast, towards an annual average of about –15°C. Indeed this value compares well with the average annual temperature of –16°C at Neumayer (Kärkäs, 2004).

Comparing our results with a similar traverse by Van den Broeke and others (1999), we find that our high potential temperature for sensor 7 on Amundsenisen is likely to be a local maximum. In their profile, a distinct maximum is seen at the edge of the interior plateau, with potential temperatures declining again towards the interior. The authors attributed this variation to locally enhanced mixing, where cold surface air locally mixes with air of higher potential temperature drawn from layers aloft. The enhanced drawdown is enabled by the downslope acceleration of the katabatic layer, creating divergence at the surface. This local anticyclonic circulation may explain, at least in part, the locally reduced net annual snow accumulation found by Van den Broeke and others (1999) near the edge of the plateau.

4.2. Time variations in temperature

Figure 7 shows the air-temperature time series for sensors 4 (altitude 905 m) and 8 (altitude 280 m). With a dry adiabatic lapse rate, the altitude difference corresponds to a 6.1°C temperature difference under neutral stratification. The timing and frequency of the twice-daily sampling has limitations when examining high-frequency temperature variations (the solar noon is within 1030 and 1130 GMT). The daily average is unbiased but the diurnal temperature amplitude is underestimated. Data from sensors 4 and 8 indicate that in summer the amplitude of the daily temperature cycle is 2–3°C but later, as insolation diminishes in March, it approaches zero. A similar daily cycle in January was also recorded at the Aboa AWS. There are differences between the daily amplitude near the coast and that further inland, but we do not have sufficiently long records from other sites to meaningfully analyse these differences.

For sensors 4 and 8, the temperature level decreases smoothly towards austral winter to around –30°C, maintaining a difference ~6°C (Fig. 7). As summer turns to autumn and winter, the differences increase, to reach a maximum by

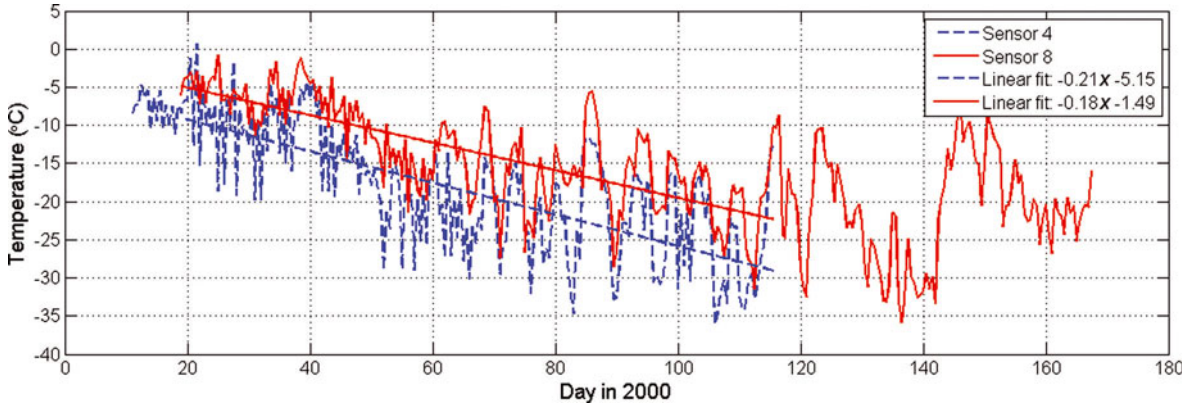

Fig. 7. Air-temperature time series at sensors 4 and 8.

https://doi.org/10.3189/002214309790794823 Published online by Cambridge University Press

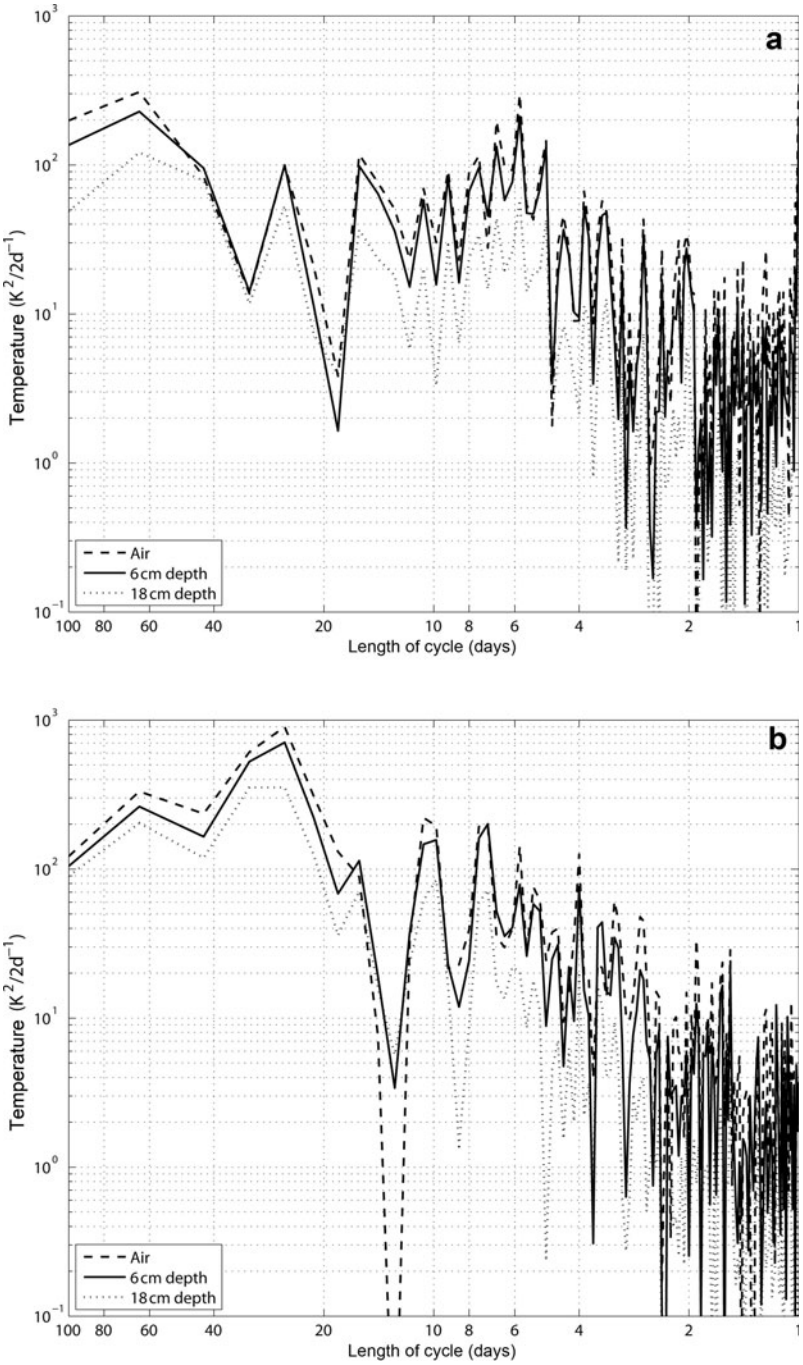

Fig. 8. Power spectra of air and snow temperature. (a) Sensor 4 from mid-January to mid-April. (b) Sensor 8 from mid-January to June.

February–March. Figure 8 shows spectra for air and snow temperatures estimated from the records for sensors 4 and 8. A broad peak is seen at the synoptic timescale. The amplitude of this component slightly increases over time as winter progresses at Kvitkuven (sensor 8), in a manner similar to that observed in meteorological data from the Neumayer meteorological station (Kärkäs, 2004).

The evolution of snow temperature, $T = T(t, z)$, follows the classical heat conduction law (e.g. Paterson, 1994). If the surface boundary conditions are $T(t, 0) = T_\infty + \Delta T \sin(2\pi\omega t)$ and $T \rightarrow T_\infty$ with $z \rightarrow \infty$, the solution is

$$T(t, z) = T_\infty + \Delta T e^{-\lambda z} \sin(2\pi\omega t - \lambda z), \quad (4)$$

where T_∞ is mean temperature, ΔT is temperature amplitude, ω is frequency and λ is a parameter which determines the attenuation and phase shift for the temperature signal:

$$1\lambda = \sqrt{\frac{\pi\omega\rho c}{k}} = \sqrt{\frac{\pi\omega}{D}}, \quad (5)$$

where c is the specific heat of ice, ρ is the density, k is the thermal conductivity and D is the heat diffusion coefficient. Thus, when the damping or phase shift at a fixed depth is known, the diffusion coefficient can be obtained and, since the density is nearly constant in the top layer, the thermal conductivity of snow can be estimated. The temperature recordings show that the e-folding depth of the 5 day cycle is 45 cm, thus $D = 1.5 \times 10^{-6}\,\mathrm{m^2\,s^{-1}}$ and taking $\rho = 400\,\mathrm{kg\,m^{-3}}$ we have $k = 1.2\,\mathrm{W\,m^{-1}\,{}^\circ C^{-1}}$.

The temperature gradient at the surface snow is proportional to the heat flux from the snow cover. In the polar

https://doi.org/10.3189/002214309790794823 Published online by Cambridge University Press

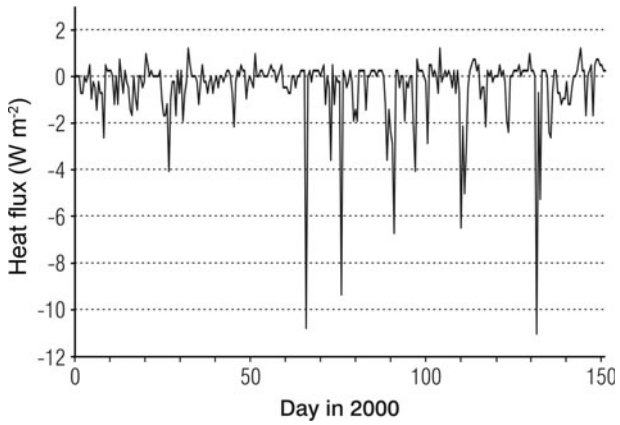

Fig. 9. Heat-flux time series estimated from the snow-temperature data at sensor 8. Negative values represent heat loss from snow cover.

night, in the absence of solar radiation, we have

$$k\frac{\partial T}{\partial z}\bigg|_{z=0} = Q_{\mathrm{L}} + Q_{\mathrm{T}}, \qquad (6)$$

where Q_{L} is net terrestrial radiation and Q_{T} is the turbulent exchange at the surface. The temperature gradient at 0.5 m depth was evaluated from the data, to represent the heat flux across the top layer of snow. The resulting heat-flux time series is shown in Figure 9. The flux was negative almost all the time, as expected. The typical level was from –2 to –1 W m^{-2}, while the peaks reached around –10 W m^{-2}.

5. CONCLUSIONS

The nine snow sensors deployed across the katabatic zone from the Amundsenisen plateau to the ice-shelf edge in Dronning Maud Land experienced major problems in the harsh Antarctic environment. Although the sensors all failed prematurely, for reasons which had not been anticipated, information about snow-cover dynamics and microclimate could be obtained from the data collected during the short period of operation and from ancillary data obtained in association with sensor deployment and retrieval.

The sensors record the temperature profile across the snow–air interface, and the change in the temperature gradient across the interface can be taken as the snow surface. This surface records also the accumulation and ablation due to the migration of snow dunes. The sensor sites, apart from Högisen ice dome, were, however, chosen from large even areas where the net influence of the migrating dunes is expected to be small over long timescales.

The net snow accumulation rates on Högisen were some five times greater than those at lower altitudes nearby. It is hypothesized that unloading of wind-blown snow is important, not only to maintain such topographic features, but also to the greater rates of snow accumulation near the coast noted by other researchers. However, we have no further evidence supporting this. The high rates of accumulation near the shelf edge appear to be related to wind redistribution rather than snowfall. This implies that the coast-to-inland precipitation gradient is less important than previously thought.

Much of the precipitation fell in autumn when we were collecting data. The main precipitation events were discrete, spaced 3–5 weeks apart with snowfall in the 30–60 mm w.e. range, declining with distance away from the sea. At 170 km inland, only three of these precipitation events were observed (due to a shorter data record), with only 20–40 mm w.e. in each storm. Snow accumulation from individual events is highly variable spatially, even over short distances. By day 160, the snow depth observed on retrieval of sensor 8 after 1 year near the coast had already been reached, supporting model results of Van Lipzig and others (2002b) that much of the snowfall in the area occurs early in the winter. More precisely, from day 160 to the end of the year, accumulation and ablation are approximately equal.

Our analysis of potential temperature shows a gradual cooling of the surface boundary layer from the edge of the interior plateau all the way to the coast. The correlation with slope suggests that evaporation of wind-blown snow is important to this cooling. The higher potential temperatures on Basen (sensor 3) and Högisen (sensor 2), with respect to the glacier below, illustrate an annual average inversion in the former case and, in the latter case, local anticyclonic drawdown, or possibly condensation in the katabatic layer as it ascends the hill.

In conclusion, the sensor concept is good, but the data-collection technology needs to be improved for a feasible system. A new effort for a larger-scale study will be made during the FINNARP 2009–12 programme in the same region, where snow sensor data will be combined with remote-sensing data and an accumulation/ablation model.

ACKNOWLEDGEMENTS

We thank fellow expedition members for good company and assistance in the field. The project was financed by the Academy of Finland (#43925 and #54086 to M. Leppäranta and a collaborative research grant to H.B. Granberg). Field logistics were provided by the Finnish Antarctic Research Program (FINNARP), and COURT Helicopters provided transport to some of the field sites.

REFERENCES

EPICA Community Members. 2004. Eight glacial cycles from an Antarctic ice core. *Nature,* **429**(6992), 623–628.

Gow, A.J. and R. Rowland. 1965. On the relationship of snow accumulation to surface topography at 'Byrd Station', Antarctica. *J. Glaciol.,* **5**(42), 843–847.

Granberg, H.B. and G.J. Irwin. 1990. A geographic snow information system for vehicle mobility prediction. *In Proceedings of the 10th International Conference of the International Society for Terrain-Vehicle Systems (ISTVS), 20–24 August 1990, Kobe, Japan. Vol. 2.* Durham, NC, International Society for Terrain-Vehicle Systems, 95–106.

Holmlund, P. and J.O. Näslund. 1994. The glacially sculptured landscape in Dronning Maud Land, Antarctica, formed by wet-based mountain glaciation and not by the present ice sheet. *Boreas,* **23**(2), 139–148.

Isaksson, E. 1992. *Spatial and temporal patterns in snow accumulation and oxygen isotopes, western Dronning Maud Land, Antarctica.* University of Stockholm, Department of Physical Geography, Stockholm. (Report STOU-NG 87.)

Isaksson, E. and W. Karlén. 1994a. High resolution climatic information from short firn cores, western Dronning Maud Land, Antarctica. *Climatic Change,* **26**(4), 421–434.

Isaksson, E. and W. Karlén. 1994b. Spatial and temporal patterns in snow accumulation, western Dronning Maud Land, Antarctica. *J. Glaciol.,* **40**(135), 399–409.

https://doi.org/10.3189/002214309790794823 Published online by Cambridge University Press

Isaksson, E., W. Karlén, N. Gundestrup, P. Mayewski, S. Whitlow and M. Twickler. 1996. A century of accumulation and temperature changes in Dronning Maud Land, Antarctica. *J. Geophys. Res.,* **101**(D3), 7085–7094.

Jonsson, S. 1988. *Observations on the physical geography and glacial history of the Vestfjella nunataks in western Dronning Maud Land, Antarctica.* University of Stockholm, Department of Physical Geography, Stockholm. (Report STOU-NG 68.)

Kanto, E., M. Leppäranta and O.-P. Mattila. 2007. Seasonal snow in Antarctica. Data report II. *Rep. Ser. Geophys.* 55.

Kärkäs, E. 2004. Meteorological conditions of the Basen Nunatak in western Dronning Maud Land, Antarctica, during the years 1989–2001. *Geophysica,* **40**(1–2), 39–52.

Kärkäs, E., H.B. Granberg, K. Kanto, K. Rasmus, C. Lavoie and M. Leppäranta. 2002. Physical properties of the seasonal snow cover in Dronning Maud Land, East Antarctica. *Ann. Glaciol.,* **34**, 89–94.

Kärkäs, E., T. Martma and E. Sonninen. 2005. Physical properties and stratigraphy of surface snow in western Dronning Maud Land, Antarctica. *Polar Res.,* **24**(1–2), 55–67.

Kotlyakov, V.M. 1966. *The snow cover of the Antarctic and its role in the present-day glaciation of the continent, ed.* B. Deutsch. Jerusalem, Israel Program for Scientific Translations.

Melvold, K., J.O. Hagen, J.F. Pinglot and N. Gundestrup. 1998. Large spatial variation in accumulation rate in Jutulstraumen ice stream, Dronning Maud Land, Antarctica. *Ann. Glaciol.,* **27**, 231–238.

Paterson, W.S.B. 1994. *The physics of glaciers. Third edition.* Oxford, etc., Elsevier.

Petit, J.R. *and 18 others*. 1999. Climate and atmospheric history of the past 420,000 years from the Vostok ice core, Antarctica. *Nature,* **399**(6735), 429–436.

Rasmus, K., H.B. Granberg, K. Kanto, E. Kärkäs, C. Lavoie and M. Leppäranta. 2003. Seasonal snow in Antarctica. *Rep. Ser. Geophys.* 47.

Reijmer, C.H. 2001. Antarctic meteorology: a study with automatic weather stations. (PhD thesis, University of Utrecht.)

Reijmer, C.H. and M.R. van den Broeke. 2003. Temporal and spatial variability of the surface mass balance in Dronning Maud Land, Antarctica, as derived from automatic weather stations. *J. Glaciol.,* **49**(167), 512–520.

Richardson, C., E. Aarholt, S.E. Hamran, P. Holmlund and E. Isaksson. 1997. Spatial distribution of snow in western Dronning Maud Land, East Antarctica, mapped by a ground-based snow radar. *J. Geophys. Res.,* **102**(B9), 20 ,343–20,353.

Richardson-Näslund, C. 2004. Spatial characteristics of snow accumulation in Dronning Maud Land, Antarctica. *Global Planet. Change,* **42**(1–4), 31–43.

Schytt, V. 1960. Glaciology II(D). Snow and ice temperatures in Dronning Maud Land. *Norwegian–British–Swedish Antarctic Expedition, 1949–52, Scientific Results* IV. Oslo, Norsk Polarinstitutt.

Van den Broeke, M.R. *and 6 others*. 1999. Climate variables along a traverse line in Dronning Maud Land, East Antarctica. *J. Glaciol.,* **45**(150), 295–302.

Van Lipzig, N.P.M., E. van Meijgaard and J. Oerlemans. 2002a. The effect of temporal variations in the surface mass balance and temperature-inversion strength on the interpretation of ice-core signals. *J. Glaciol.,* **48**(163), 611–621.

Van Lipzig, N.P.M., E. van Meijgaard and J. Oerlemans. 2002b. The spatial and temporal variability of the surface mass balance in Antarctica: results from a regional climate model. *Int. J. Climatol.,* **22**(10), 1197–1217.

MS received 22 September 2008 and accepted in revised form 14 October 2009